International Journal of Multiphase Flow 34 (2008) 987–995

Contents lists available at ScienceDirect

International Journal of Multiphase Flow

journal homepage: www.elsevier.com/locate/ijmulflow

Diffuse-interface modeling of phase segregation in liquid mixtures

A.G. Lamorgese [a,*], R. Mauri [b]

[a] Center for Turbulence Research, Stanford University, Stanford, CA 94305-3035, USA
[b] Department of Chemical Engineering, Industrial Chemistry and Material Science, Università di Pisa, 56126 Pisa, Italy

ARTICLE INFO

Article history:
Received 6 November 2007
Available online 25 March 2008

Keywords:
Two-phase flow
Phase transition
Computational fluid dynamics

ABSTRACT

We simulate the phase separation of a binary mixture that is deeply quenched into the unstable range of its phase diagram. The mixture is described through the diffuse-interface model and the governing equations are integrated in 2D and 3D in a periodic box and in a channel using a pseudo-spectral method. Spinodal decomposition patterns for critical and off-critical mixtures are studied, revealing the scaling laws of the characteristic lengthscale and composition of single-phase microdomains, together with their dependence on the Peclet number. Comparison between 2D and 3D results reveals that 2D simulations capture, even quantitatively, the main features of the phenomenon. However, while the agreement between 2D and 3D simulations is excellent when the mixture is confined in a periodic box, it appears to be less pronounced in a channel-like geometry.

1. Introduction

Spinodal decomposition of deeply quenched binary mixtures has been the subject of many theoretical, numerical and experimental investigations. Reviews on spinodal decomposition can be found in Langer (1980) and in Gunton et al. (1983). It is well known that any unstable system is best studied assuming that it is perturbed through a delocalized, infinitesimal fluctuation (Beretta and Gyftopoulos, 2005). In this case, in fact, the problem can be linearized for short times, showing that the intensity of any mode whose wavelength is larger than a critical value grows exponentially in time, with the maximum growth corresponding to the typical lengthscale of the process. Theoretically, this idea is best brought to fruition using the diffuse-interface model (Antanovskii, 1995, 1996; Lowengrub and Truskinovsky, 1998; Anderson et al., 1998) (also known as Model H, in the taxonomy of Hohenberg and Halperin (1977), which is based on the pioneering work by Van der Waals (1894) and the Ginzbug–Landau theory of phase transition (Landau and Lifshitz, 1953; Le Bellac, 1991). This approach was employed by Cahn and Hilliard (1958, 1959) and Horvay and Cahn (1961) to investigate diffusion-driven spinodal decomposition and nucleation and was later generalized to include hydrodynamics by Kawasaki (1970), Siggia (1979) and others, who included into the Navier–Stokes equations the Korteweg force, i.e. a non-equilibrium body force, driven by chemical potential gradients.

Initially, spinodal decomposition is characterized by the exponential growth of all disturbances in the composition field, which gives rise to single-phase microdomains whose size corresponds to the fastest growing mode of the linear regime (Mauri et al., 1996). At this point, material transport can occur either by diffusion or by convection. In cases where diffusion is the only transport mechanism, both analytical calculations (Lifshitz and Pitaevskii, 1984) and dimensional analysis (Siggia, 1979) predict a growth law $\mathscr{L}(t) \sim t^{1/3}$ for the characteristic size of single-phase microdomains. On the other hand, when hydrodynamic interactions are important, as is the case with low-viscosity liquid mixtures, the effect of the convective mass flow due to chemical potential gradients cannot be neglected. In this case, both dimensional analysis (Siggia, 1979) and numerical simulation (Vladimirova et al., 1998, 1999a,b; Lamorgese and Mauri, 2005) show that $\mathscr{L}(t) \sim t$, thus confirming experimental results (Guenoun et al., 1987; Gupta et al., 1999; Poesio et al., 2006). Finally, the coarsening process in the inertial regime and the effects of turbulent stirring on phase separation have been addressed in other works (Furukawa, 1985; Kendon, 2000; Kendon et al., 2001; Berti et al., 2005).

In this work, we investigate three-dimensional spinodal decomposition patterns of critical and off-critical regular binary mixtures at low Reynolds number. Numerical simulations of 3D spinodal decomposition of fluid mixtures have been carried out in the past, first by Valls and Farrell (1993) and, then, by others (Caneba et al., 2002; Badalassi et al., 2003; Prusty et al., 2007). In none of these works any major difference between 2D and 3D simulations was reported, although they all stress that more effort is needed, since these previous simulations have been carried out in relatively small 3D boxes. To circumvent this problem, we have developed a parallel pseudo-spectral code, validated it by considering a test case and then we employed it to compare 2D and 3D results.

* Corresponding author. Tel.: +1 650 725 1821; fax: +1 650 725 3525.
E-mail address: AG17@STANFORD.EDU (A.G. Lamorgese).

0301-9322/$ - see front matter © 2008 Elsevier Ltd. All rights reserved.
doi:10.1016/j.ijmultiphaseflow.2008.03.003

This article is organized as follows. In Section 2 and 3, the governing equations and the numerical approach are briefly outlined. Then, in Section 4, first the code is validated by simulating phase separation in the metastable range, comparing our predictions with well known results. Finally, the spinodal decomposition patterns and the scaling law for the typical domain size in the viscous regime are discussed. At the end, a few conclusions are drawn.

2. The governing equations

Under isothermal conditions, the motion of a regular binary mixture (where the two components are assumed to have equal densities, viscosities and molecular weights) at low Reynolds number is described by the generalized Cahn–Hilliard and Stokes equations (Lamorgese et al., 2002, 2005, 2006):

$$\partial_t \phi + \nabla \cdot \phi \mathbf{u} = -\nabla \cdot \mathbf{J}_\phi, \tag{1}$$

$$\nabla p = \eta \nabla^2 \mathbf{u} + \mathbf{F}_\phi, \tag{2}$$

$$\nabla \cdot \mathbf{u} = 0. \tag{3}$$

Here, $\mathbf{u}$ is the mass-averaged velocity, ϕ is the mass fraction, $\mathbf{J}_\phi$ is the diffusive (or antidiffusive) volume flux, and $\mathbf{F}_\phi$ is the Korteweg force. These last two terms are the characterizing feature of the diffuse-interface model. In particular, $\mathbf{J}_\phi$ is proportional to the gradient of the chemical potential difference through the relation (Mauri et al., 1996; Vladimirova et al., 1998)

$$\mathbf{J}_\phi = -\phi(1-\phi) D \nabla \tilde{\mu}, \tag{4}$$

where D is the molecular diffusivity and $\tilde{\mu}$ the chemical potential difference, defined as $\tilde{\mu} = \delta(\tilde{g}/RT)/\delta\phi$. Here, $\tilde{g}$ denotes the molar Gibbs free energy of mixing for a non-homogeneous mixture at temperature T and pressure P (Cahn and Hilliard, 1958):

$$\tilde{g} = RT[\phi \log \phi + (1-\phi)\log(1-\phi)] + RT\Psi\phi(1-\phi) + \frac{1}{2} RT a^2 (\nabla\phi)^2, \tag{5}$$

R being the universal gas constant. In Eq. (5), a is a characteristic microscopic length, while Ψ is the Margules parameter, which describes the repulsive interaction between unlike molecules vs. that between like molecules. Whenever the mixture is brought from the single-phase to the two-phase region of its phase diagram, phase separation occurs, ending with two coexisting phases separated by a sharp interface. At this point, a surface tension σ can be defined and measured and from that, as shown by Van der Waals (1894), a can be determined as

$$a \sim \frac{1}{\sqrt{\tau}(\Delta\phi)_{\mathrm{eq}}^2} \frac{\sigma M_{\mathrm{W}}}{\rho RT}, \tag{6}$$

where $(\Delta\phi)_{\mathrm{eq}}$ is the composition difference between the two phases at equilibrium, M_{W} is the molecular weight, while $\tau = (\Psi - \Psi_{\mathrm{c}})/\Psi_{\mathrm{c}}$, where $\Psi_{\mathrm{c}} = 2$ is the critical value of Ψ.

The Korteweg force appearing in Eq. (2) can also be defined from thermodynamic considerations. In fact, using Hamilton's principle (and therefore neglecting all dissipative terms), $\mathbf{F}_\phi$ can be shown to be equal to the generalized gradient of the free energy (Lowengrub and Truskinovsky, 1998; Lamorgese and Mauri, 2006),

$$\mathbf{F}_\phi = \frac{\rho}{M_{\mathrm{W}}} \frac{\delta \tilde{g}}{\delta \mathbf{r}} = \frac{\rho RT}{M_{\mathrm{W}}} \tilde{\mu} \nabla \phi. \tag{7}$$

In particular, at the late stages of phase separation, after the system has developed well-defined phase interfaces, this body force reduces to the more conventional surface tension (Jasnow and Vinals, 1996; Jacqmin, 2000). Therefore, being proportional to $\tilde{\mu} = \mu_A - \mu_B$, which is identically zero at local equilibrium, $\mathbf{F}_\phi$ can be thought of as a non-equilibrium capillary force. It should be stressed that local equilibrium (where the concentration of the drops and that of the surrounding continuous phase equal their equilibrium values) is reached only well after sharp interfaces are formed. In fact, as observed by Santonicola et al. (2001), microdomains continue to move rapidly well after they have developed sharp interfaces.

Since $\mathbf{F}_\phi$ is driven by surface energy, it tends to minimize the energy stored at the interface driving, say, A-rich drops towards A-rich regions. The resulting non-equilibrium attractive force f_A between two isolated drops of radius r separated by a thin film of thickness ℓ can be easily evaluated as $f_A \sim F_\phi r^2 \ell \sim \sqrt{\tau} r^2 \sigma / a$, where $F_\phi \sim \sigma/\ell^2$ can be obtained from Eqs. (6) and (7). This value is much larger than that of any repulsive interaction among drops due to the presence of surface-active compounds, thus explaining why the rate of phase separation in deeply quenched liquid mixtures is almost independent of the presence of surfactants (Gupta et al., 1999).

The ratio between the convective and diffusive mass fluxes defines the Peclet number, $N_{Pe} = Va/D$, where V is a characteristic velocity, which can be estimated through (2) and (7) as $V \sim F_\phi a^2/\eta$, with $F_\phi \sim \rho RT/(aM_{\mathrm{W}})$. Finally we obtain,

$$N_{Pe} = \alpha\sqrt{\tau}, \quad \text{where } \alpha = \frac{a^2}{D}\frac{\rho}{\eta}\frac{RT}{M_{\mathrm{W}}}. \tag{8}$$

α coincides with the "fluidity" parameter defined by Tanaka and Araki (1998). For systems with very large viscosities, α is small and the model describes a diffusion-driven phase separation process, as in polymer melts and alloys (Mauri et al., 1996). For most liquids, however, α is very large, typically $\alpha > 10^3$, showing that diffusion is important only at the very beginning of the separation process, in that it creates a non-uniform concentration field. Then, the concentration gradients within the system will drive the subsequent convection, which, as it happens, becomes the dominant mechanism for mass transport until drops become large enough (typically of O(1 mm)) that gravity takes over. On the other hand, for quasi critical mixtures, with $\tau \sim 0$, the Korteweg force (and therefore the Peclet number as well) vanishes, so that diffusion becomes the dominant mechanism of phase segregation. Although this approach has been derived for very idealized systems, it seems to capture the main features of real mixtures, at least during the phase separation process. That is why we did not add further terms to generalize our model, although they can be derived rather easily (Vladimirova et al., 1998, 1999a,b).

3. Numerical methods

3.1. Periodic box geometry

The governing Eqs. (1)–(3) (in dimensionless form) can be rewritten as follows:

$$(\partial_t - \nabla^2)\phi = -\nabla^2\left\{\phi(1-\phi)\left[2\Psi\phi + \left(\frac{a}{L}\right)^2 \nabla^2\phi\right]\right\} + \nabla\cdot\left\{\left[2\Psi\phi + \left(\frac{a}{L}\right)^2\nabla^2\phi\right](1-2\phi)\nabla\phi - \alpha\phi\mathbf{u}\right\}, \tag{9}$$

$$\left(\frac{a}{L}\right)^2 \nabla^2 \mathbf{u} = \mathbb{P}(\nabla)\phi\nabla\tilde{\mu}, \quad \mathbb{P}_{ij}(\nabla) := \delta_{ij} - \nabla^{-2}\partial_{ij}^2, \tag{10}$$

where all lengths and times are scaled by L and L^2/D, respectively, with L denoting a macro lengthscale, which in our case coincides with the periodicity length of the computational domain. The projector $\mathbb{P}(\nabla)$ guarantees that the velocity is solenoidal at all times. Accordingly, Eq. (10) can be seen as a "static" constraint on the (nondimensional) velocity field, i.e., at each instant in time the velocity can be determined once the concentration field is known (so that the $\mathbf{u}$-dependence on the RHS of Eq. (9) can be formally dropped). Although periodic boundary conditions enable a straightforward pseudo-spectral discretization of the equations, special

care must be taken to avoid aliasing errors in the computation of nonlinear terms.

Quadratic nonlinearities are usually made alias-free using the so-called padding method (Canuto et al., 1988), consisting of collocating in physical space on a refined grid with $(3/2)^3$ as many grid points as the number of active modes N^3 in the calculation. Using the padding method, a refined grid of $(2N)^3$ points is required for dealiasing the cubic nonlinearities. In our production runs (with 256^3 grid points), the '3/2 rule' was employed for both quadratic and cubic nonlinearities since the remaining aliasing errors were found to be negligible. Dealiasing by the '3/2 rule' was implemented in our code using the parallel strategy shown by Iovieno et al. (2001).

The Fourier-transformed system can be written in the form:

$$\frac{\mathrm{d}}{\mathrm{d}t}[\mathrm{e}^{k^2 t}\hat{\phi}(\mathbf{k},t)] = \mathrm{e}^{k^2 t}\widehat{N}(\mathbf{k},t), \tag{11}$$

where the Fourier coefficients are denoted by hats, and an integrating factor has been employed for the 'exact' treatment of the purely diffusive term on the LHS of (9). The grid spacing is such that interface profiles are resolved with three collocation points, i.e., $\Delta x = a/2$. Eq. (11) is time-integrated using the standard fourth-order Runge–Kutta scheme, with a variable time step Δt determined by the Courant–Friedrichs–Lewy condition,

$$\Delta t = N_{\mathrm{C}}\frac{\Delta x}{V}, \tag{12}$$

where Δx is the dimensionless grid spacing, N_{C} is the Courant number, and V is a characteristic dimensionless bulk velocity. In our case, considering that convection is induced by concentration gradients, we have assumed that $V = \max[|\phi_x| + |\phi_y| + |\phi_z|]$, where max indicates the maximum attained over all of the collocation points, so that at each time step the advancement scheme is sensitive to the spatial gradients of ϕ. The Courant number is chosen such that the time-advancement scheme is numerically stable and the smallest dynamical motions are accurately computed. Unfortunately, the nonlinearity of the equation prevents a rigorous determination of the stability limit and imposes a trial-and-error determination of the maximum acceptable Courant number. In our simulations, we chose $N_{\mathrm{C}} = N_{\mathrm{C}}^*(\alpha)$ (with $N_{\mathrm{C}}^*(\alpha) = 0.01$–$0.1$ depending on the given value for α) as we found that when $N_{\mathrm{C}} > N_{\mathrm{C}}^*(\alpha)$ the scheme can be numerically unstable. Note that, having used the integrating factor, there is no concern for the viscous stability of the scheme for any values of the Courant number. Two types of initial conditions were considered.

(1) A random (white-in-space) noise superposed on a constant field ϕ_0,

$$\hat{\phi}_{\mathbf{k}}(0) = \phi_0\delta_{\mathbf{k},\mathbf{0}} + \frac{1}{N}\tilde{\phi}\mathrm{e}^{\mathrm{i}\theta}, \tag{13}$$

where θ is a different uniform deviate in $[0, 2\pi]$ for each wave vector $\mathbf{k}$ subject to the requirement of Hermitian symmetry of the Fourier coefficient, whereas $\tilde{\phi}$ controls the magnitude of the white-noise component.

(2) An isolated drop, centered at the origin, with composition

$$\phi(\mathbf{r}) = \begin{cases} \phi_{\mathrm{eq}}^{\mathrm{I}}, & \text{if } |\mathbf{r}| \leqslant R_0 - a, \\ \phi_{\mathrm{b}} + \frac{1}{2}\{\phi_{\mathrm{eq}}^{\mathrm{I}} - \phi_{\mathrm{b}}\}\left[1 + \cos\frac{\pi}{a}(|\mathbf{r}| - R_a + a)\right], & \text{if } R_0 - a < |\mathbf{r}| \leqslant R_0, \\ \phi_{\mathrm{b}}, & \text{if } |\mathbf{r}| > R_0, \end{cases} \tag{14}$$

where R_0 is the radius of the drop, while ϕ_{b} is the background composition, calculated so as to satisfy the constraint of a prescribed average value $\hat{\phi}_0 = \phi_0$. In fact, it can be shown that

$$\phi_{\mathrm{b}} = \left[\phi_0 - \frac{2}{3\pi}\left(\frac{a}{L}\right)^3(2\rho - 1)[\pi^2(\rho^2 - \rho + 1) - 6]\phi_{\mathrm{eq}}^{\mathrm{I}}\right] \times \left[1 - \frac{2}{3\pi}\left(\frac{a}{L}\right)^3(2\rho - 1)[\pi^2(\rho^2 - \rho + 1) - 6]\right]^{-1}, \tag{15}$$

where $\rho = R_0/a$.

3.2. Channel-like geometry

We now describe numerical methods to integrate Eqs. (1)–(3) in a channel-like geometry. Fourier pseudo-spectral methods are used to discretize the streamwise (x) and spanwise (z) directions, whereas fourth-order compact finite differences (Lele, 1992) are applied to the wall-normal (y) direction. The equations are made dimensionless, with all lengths and times scaled by h and h^2/D, respectively, with h denoting the channel half-width. After Fourier-transforming in the x and z directions, the Cahn–Hilliard equation (Eq. (9)) can be rewritten as follows:

$$\frac{\mathrm{d}}{\mathrm{d}t}[\mathrm{e}^{f(k)t}\hat{\phi}_{\mathbf{k}}(y,t)] = \mathscr{L}(k)\mathrm{e}^{f(k)t}\hat{\phi}_{\mathbf{k}}(y,t) + \mathrm{e}^{f(k)t}\widehat{N}_{\mathbf{k}}(y,t), \tag{16}$$

where

$$f(k) := (1 - 2\Psi\beta_h)|\mathbf{k}|^2 + \beta_h\left(\frac{a}{h}\right)^2|\mathbf{k}|^4, \tag{17}$$

$$\mathscr{L}(k) := \left[1 - 2\Psi\beta_h + 2\beta_h|\mathbf{k}|^2\left(\frac{a}{h}\right)^2\right]D_2 - \beta_h\left(\frac{a}{h}\right)^2 D_4, \tag{18}$$

$$N := -\nabla^2\left\{[\phi(1-\phi) - \beta_h][2\Psi\phi + \left(\frac{a}{h}\right)^2\nabla^2\phi]\right\} + \nabla\cdot\left\{[2\Psi\phi + \left(\frac{a}{h}\right)^2\nabla^2\phi](1 - 2\phi)\nabla\phi - \alpha\phi\mathbf{u}\right\}. \tag{19}$$

Here, D_2 and D_4 denote second- and fourth-order differentiation matrices (from the compact finite-difference discretization), whereas β_h is a numerical hyperdiffusivity (discussed further below). For the Cahn–Hilliard equation, the following wall-boundary conditions are imposed: (i) a no-flux condition $\mathbf{J}_\phi\cdot\mathbf{n} = 0$ at $y = \pm 1$, and (ii) a wetting condition. The latter is the result of modeling assumptions for the surface Gibbs free energy integral

$$-\int g_s(\phi, \nabla\phi)\mathrm{d}S_{\mathrm{w}}, \tag{20}$$

that needs to be included in the Lagrangian when the non-dissipative dynamics of the system is considered (Lamorgese and Mauri, 2006). In the present simulations, a simple local model is employed (Jacqmin, 2000), i.e.,

$$g_s(\phi) = \sigma_{B,\mathrm{w}} + (\sigma_{A,\mathrm{w}} - \sigma_{B,\mathrm{w}})\phi, \tag{21}$$

where $\sigma_{A,\mathrm{w}}$ and $\sigma_{B,\mathrm{w}}$ denote surface tensions between A and the wall and B and the wall, respectively. The resulting wall-boundary conditions require that the normal derivative of ϕ be proportional to the difference $(\sigma_{A,\mathrm{w}} - \sigma_{B,\mathrm{w}})$. For simplicity, in the simulations shown below the additional assumption $\sigma_{A,\mathrm{w}} = \sigma_{B,\mathrm{w}}$ is employed. In summary, the following wall-boundary conditions for the Cahn–Hilliard equation are imposed:

$$\frac{\partial\phi}{\partial y} = 0, \quad \frac{\partial^3\phi}{\partial y^3} = 0. \tag{22}$$

In our solution algorithm, these are implemented using an influence-matrix technique (Canuto et al., 1988).

The Cahn–Hilliard equation is integrated in time using a second-order Runge–Kutta/Crank–Nicolson technique (Peyret, 2000). The application of this semi-implicit temporal scheme requires that the linear operator $\mathscr{L}$ be a fourth-order differential operator.

This is not the case with the Cahn–Hilliard equation (Eq. (9)) because the biharmonic term has a factor with a nonlinear ϕ-dependence. However, by means of β_h the linear operator $\mathscr{L}$ includes a fourth-order derivative, so as to render enforcement of boundary conditions for ϕ possible. In numerical experiments, a stable and accurate temporal advancement is obtained with $|\beta_h| \leqslant 5 \times 10^{-6}$ (in our production runs we used $\beta_h = 5 \times 10^{-6}$). With $|\beta_h| \leqslant 5 \times 10^{-6}$, $\langle\phi\rangle$ is conserved to five significant digits and the separation statistics (e.g., the separation depth) are insensitive to values of β_h in that range.

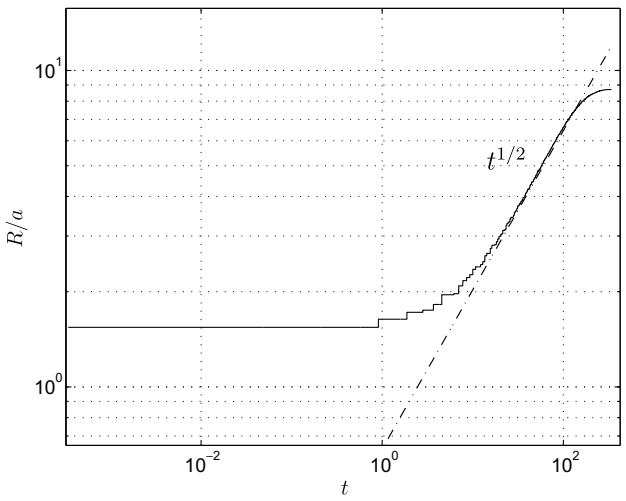

Fig. 1. Drop radius R/a vs. nondimensional time for an isolated nucleating drop with $\phi_0 = 0.35$, $\Psi = 2.1$, $\alpha = 0$.

To solve the Stokes equation we use a vertical-velocity/vertical-vorticity formulation (as in Kim et al. (1987)). We first take the curl of Eq. (2), which eliminates the pressure and yields a "static" equation for the vorticity $\boldsymbol{\omega}$:

$$\nabla^2\boldsymbol{\omega} = -\nabla\phi \times \nabla\nabla^2\phi. \tag{23}$$

Taking the curl once more yields

$$\nabla^4\mathbf{u} = \nabla \times (\nabla\phi \times \nabla\nabla^2\phi). \tag{24}$$

Since the contact line at the top and bottom walls of the domain ($y = \pm 1$) is diffuse, no-slip, no-penetration boundary conditions are appropriate for the velocity there. With no-slip, no-penetration boundary conditions at the channel walls, we have homogeneous Dirichlet boundary conditions at the walls for the wall-normal vorticity (η). Therefore, the solution of the Stokes equation is obtained by first solving the following boundary-value problems:

$$\begin{cases} (D^2 - |\mathbf{k}|^2)\hat{\eta}_{\mathbf{k}} = -\widehat{Y}_{\mathbf{k}}, \\ \hat{\eta}_{\mathbf{k}}(\pm 1) = 0, \end{cases} \tag{25}$$

and

$$\begin{cases} (D^4 - 2|\mathbf{k}|^2 D^2 + |\mathbf{k}|^4)\hat{v}_{\mathbf{k}} = \widehat{\mathscr{Y}}_{\mathbf{k}}, \\ \hat{v}_{\mathbf{k}}(\pm 1) = 0, \quad D\hat{v}_{\mathbf{k}}(\pm 1) = 0, \end{cases} \tag{26}$$

for each wavevector $\mathbf{k} = (k_x, k_z) \neq 0$. In these equations, Y denotes the y-component of $\mathbf{N} = \nabla\phi \times \nabla\nabla^2\phi$ whereas $\mathscr{Y}$ denotes the y-component of $\nabla \times \mathbf{N}$. For each $\mathbf{k} \neq 0$, the horizontal velocity components follow from continuity:

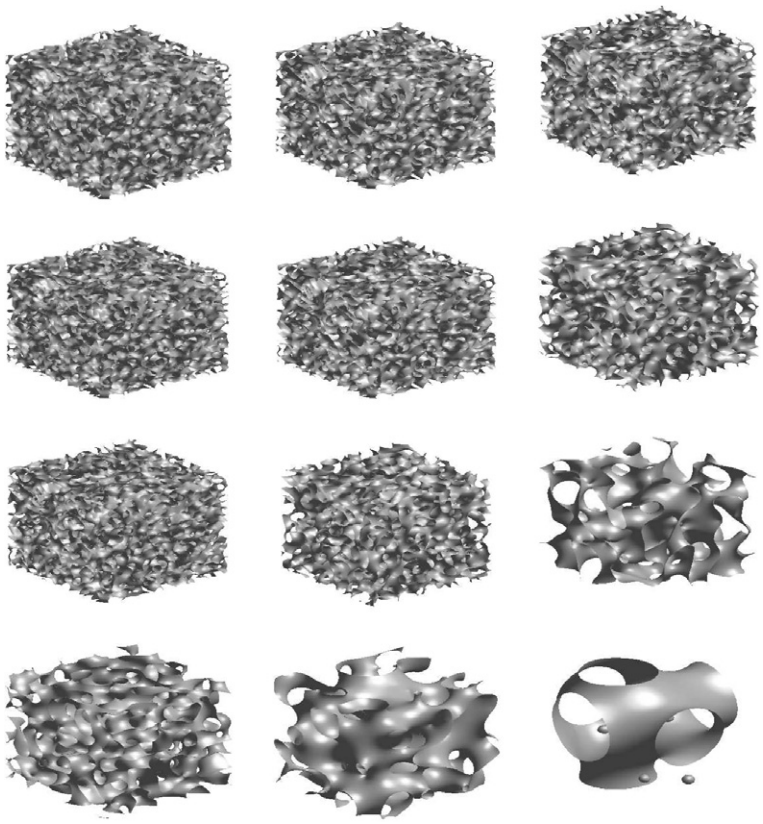

Fig. 2. Phase separation of a critical mixture (from 256^3 simulations with $\phi_0 = 0.5$ and $\Psi = 2.1$) in a periodic box at different nondimensional times $t = 0.5$, 1 and 2, with $\alpha = 0$, 10, 10^2 and 10^3 from top to bottom.

$$\hat{u}_{\mathbf{k}} = \frac{1}{|\mathbf{k}|^2}[\mathrm{i}k_x D\hat{v}_{\mathbf{k}} - \mathrm{i}k_z\hat{\eta}_{\mathbf{k}}], \tag{27}$$

$$\hat{w}_{\mathbf{k}} = \frac{1}{|\mathbf{k}|^2}[\mathrm{i}k_z D\hat{v}_{\mathbf{k}} + \mathrm{i}k_x\hat{\eta}_{\mathbf{k}}]. \tag{28}$$

Finally, the Fourier coefficients for $|\mathbf{k}| = 0$ are obtained from the following boundary-value problems:

$$\begin{cases} D^2\langle u\rangle = \overline{P}_{,x} - \left(\frac{h}{a}\right)^2\langle\tilde{\mu}\partial_x\phi\rangle, \\ \langle u\rangle(\pm 1) = 0, \end{cases} \tag{29}$$

and

$$\begin{cases} D^2\langle w\rangle = \overline{P}_{,z} - \left(\frac{h}{a}\right)^2\langle\tilde{\mu}\partial_z\phi\rangle, \\ \langle w\rangle(\pm 1) = 0, \end{cases} \tag{30}$$

where $\langle\cdot\rangle$ denotes spatial averaging over an (x,z) plane. Since our focus is on the motion induced by the phase transition, at each time step the mean pressure gradients in Eqs. (29), (30) are obtained from the relations:

$$\overline{P}_{,x} = \frac{1}{2}\left\{\left.\frac{\partial\langle u\rangle}{\partial y}\right|_{-1}^{1} + \left(\frac{h}{a}\right)^2\int_{-1}^{1}\langle\tilde{\mu}\partial_x\phi\rangle\mathrm{d}y\right\}, \tag{31}$$

$$\overline{P}_{,z} = \frac{1}{2}\left\{\left.\frac{\partial\langle w\rangle}{\partial y}\right|_{-1}^{1} + \left(\frac{h}{a}\right)^2\int_{-1}^{1}\langle\tilde{\mu}\partial_z\phi\rangle\mathrm{d}y\right\}. \tag{32}$$

Incidentally, this is the mean pressure-gradient for constant steady-state flow rate that results from the full Navier–Stokes equations.

The nonlinear terms on the RHS of Eqs. (25) and (26) would normally require nine FFTs for their pseudo-spectral evaluation. However, using the following identity,

$$(\nabla\phi\times\nabla\nabla^2\phi)_i = \partial^2_{jk}(\phi_j^2 - \phi_{,k}^2) + (\partial_k^2 - \partial_j^2)\phi_{,j}\phi_{,k} - \partial^2_{ij}\phi_{,i}\phi_{,k} + \partial^2_{ik}\phi_{,i}\phi_{,j}, \tag{33}$$

where $\{i,j,k\}$ is any cyclic permutation of $\{1,2,3\}$, their computation requires only *eight* FFTs.

Recently, Badalassi et al. (2003) have simulated phase separation in a channel using a very similar spatial discretization combined with a semi-implicit time-advancement scheme. However, being based on a direct discretization of the Navier–Stokes (or Stokes) equation, their solution algorithm requires a pressure Poisson solver. In contrast, the vertical-velocity/vertical-vorticity formulation achieves even greater efficiency as there is no need to solve for the pressure.

As mentioned above, Eq. (16) is time-integrated using a hybrid implicit/explicit integration scheme. The nonlinear term is treated explicitly with a second-order Runge–Kutta method, while the purely diffusive and hyperdiffusive terms are handled using a Crank–Nicolson scheme. As for the periodic box geometry, the time step Δt is determined by the CFL condition (12), where Δx is the dimensionless grid spacing in the x-direction and $V = \max_{y_j} V(y_j)$, with $V(y_j) = \max_{x,z}[|\phi_x| + \frac{\Delta x}{y_{j+1}-y_j}|\phi_y| + \frac{\Delta x}{\Delta z}|\phi_z|]$ and $\max_{x,z}$ indicating the maximum attained over all of the collocation points in an (x,z) plane. In our simulations, we chose $N_C = N_C^*(\alpha)$ (with $N_C^*(\alpha) = 0.001$–0.01 depending on the chosen α) as we found values of $N_C > N_C^*(\alpha)$ such that the scheme is numerically unstable.

The initial condition for ϕ in the channel-like geometry is a Gaussian white noise with a y-dependent amplitude $\phi_\epsilon(y) = \frac{\phi_\epsilon}{2}(1+\cos(\pi y))$ superposed on a uniform composition field $\phi = \phi_0$.

4. Results

4.1. Periodic box geometry

Numerical results from simulations in a periodic box are now described. The simulations were carried out in a box of size $\frac{N}{2}a$. We used $\Psi = 2.1$ because that is the value of the Margules parameter for the water–acetonitrile–toluene mixture at ambient temperature that was used in the experimental study of Gupta et al. (1999). First, we ran a test to validate our pseudo-spectral code against reference data. To do that, a uniform and very viscous

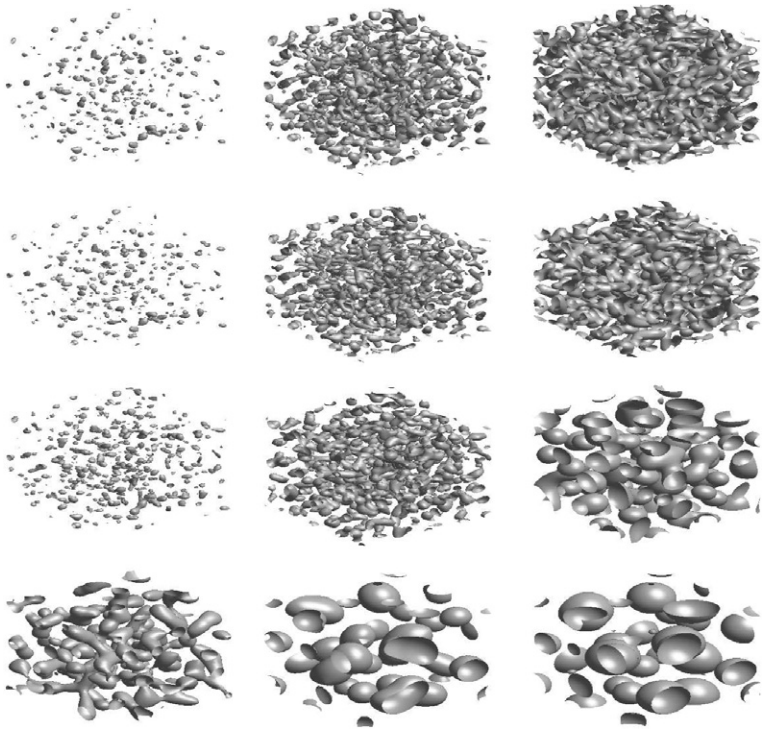

Fig. 3. Phase separation of an off-critical mixture (from 256^3 simulations with $\phi_0 = 0.45$ and $\Psi = 2.1$) in a periodic box at different nondimensional times $t = 0.5$, 1 and 2, with $\alpha = 0$, 10, 10^2 and 10^3 from top to bottom.

(i.e. for $\alpha = 0$) mixture in the metastable range of its phase diagram was perturbed by placing an isolated nucleus of the minority phase at the center of the computational domain. As expected, at first (i.e. before the solute depleted layer around the growing droplet reaches the boundary of the computational domain) the coarsening mechanism proceeds through the diffusion of the solute from the supersaturated background to the growing nucleus ("free growth") with a $t^{1/2}$ growth law (see Fig. 1), in agreement with both theoretical (Langer and Schwartz, 1980) and experimental (Colombani and Bert, 2004) results. Note that, instead, using the same approach, we have shown (Lamorgese and Mauri, 2005) that during homogeneous nucleation (i.e. when the nucleating drops "see" each other) we obtain a $t^{1/3}$ growth law, as expected (Gunton, 1999).

Next, we studied spinodal decomposition. In Figs. 2 and 3, typical surfaces with constant ϕ are shown for the critical (i.e $\phi_0 = 0.5$) and off-critical (i.e $\phi_0 = 0.45$) cases, without convection (i.e. $\alpha = 0$) and with convection, for $\alpha = 10$, 100, 1000, using a 256^3 grid. As expected, while critical mixtures phase separate by forming bicontinuous structures, the morphology of off-critical systems is composed of spherical nuclei. Then, we investigated the extent to which such results on spinodal decomposition in 3D differ from those in 2D, which have been presented previously (Lamorgese et al., 2002). To this end, we studied the rate of coarsening as reflected in the growth law for the integral scale of the radial pair-correlation function,

$$\mathscr{C}(r;t) = \frac{1}{4\pi\phi_{\mathrm{rms}}^2}\int \langle\tilde{\phi}(\mathbf{x}+\mathbf{r})\tilde{\phi}(\mathbf{x})\rangle \mathrm{d}\Omega. \tag{34}$$

The lengthscale in question can be expressed as:

$$\mathscr{L}(t) = \frac{1}{\phi_{\mathrm{rms}}^2}\sum_{\mathbf{k}}\frac{\langle|\hat{\tilde{\phi}}_{\mathbf{k}}|^2\rangle}{|\mathbf{k}|}, \tag{35}$$

where $\tilde{\phi} = \phi - \langle\phi\rangle$, ϕ_{rms} is the *rms* value of ϕ, hats denote Fourier transforms, while the brackets indicate averaging over a shell in Fourier space at fixed $k = |\mathbf{k}|$.

The solid lines in Fig. 4 represent how $\mathscr{L}/L$ varies in time in 3D simulations on a 256^3 grid, compared to the results from 2D simulations (dotted lines) on a 512^2 grid. As expected, the power-law scaling coefficient may vary from 1/3 (diffusion controlled) to 1 (hydrodynamics controlled), corresponding to cases with $\alpha = 0$ and $\alpha \gg 1$, respectively. The two sets of curves show that there is a remarkable quantitative agreement between 3D and 2D simulations.

A quantitative characterization of the influence of the Peclet number N_{Pe} on the average phase composition within the phase domains is provided by the separation depth s, measuring the "distance" of the single-phase domains from their equilibrium state, i.e.,

$$s = \left\langle \frac{\phi(\mathbf{r}) - \phi_0}{\phi_{\mathrm{eq}}(\mathbf{r}) - \phi_0} \right\rangle, \tag{36}$$

where ϕ_0 is the initial composition, and the bracket indicates volume and ensemble averaging. Here, ϕ_{eq} is the steady state composition of the A-rich phase, ϕ_{eq}^A, or the B-rich phase, ϕ_{eq}^B, depending on the local composition $\phi(\mathbf{r})$,

$$\phi_{\mathrm{eq}}(\mathbf{r}) = \phi_{\mathrm{eq}}^A, \quad \phi(\mathbf{r}) > \phi_0, \tag{37}$$

$$\phi_{\mathrm{eq}}(\mathbf{r}) = \phi_{\mathrm{eq}}^B, \quad \phi(\mathbf{r}) < \phi_0. \tag{38}$$

Accordingly, $s = 0$ initially, while $s = 1$ at local equilibrium. In Fig. 5 separation depth results from 3D simulations (solid lines) are compared with the corresponding 2D simulations. Even in this case, the two sets of results show a remarkable quantitative agreement.

4.2. Channel-like geometry

A computational domain of size $L_x = \pi Na$, $L_y = (N+1)a$, $L_z = \pi Na$ was used, with $N = 64$. Figs. 6 and 7 show $\phi = 0.5$ isosurfaces of concentration for critical and off-critical mixtures in a channel geometry. The phase ordering process is characterized by the formation of string-like structures that are aligned in a direction orthogonal to the walls. These filaments span the entire channel width for the critical mixtures, whereas prolate spheroidal drops are formed for the off-critical mixtures. The extent to which the numerical results in 3D differ from their 2D counterparts is investigated with reference to the mean integral scale for the plane-averaged pair-correlation function, given by

$$\mathscr{L} = \frac{1}{2}\int_{-1}^{1}\mathrm{d}y\,\frac{1}{\phi_{\mathrm{rms}}(y)^2}\sum_{\mathbf{k}}\frac{\langle|\hat{\phi}_{\mathbf{k}}|^2\rangle}{|\mathbf{k}|}, \tag{39}$$

and shown in Fig. 8. This figure shows remarkable quantitative agreement between the two sets of curves. However, this only holds to a lesser extent for the separation depth (Fig. 9).

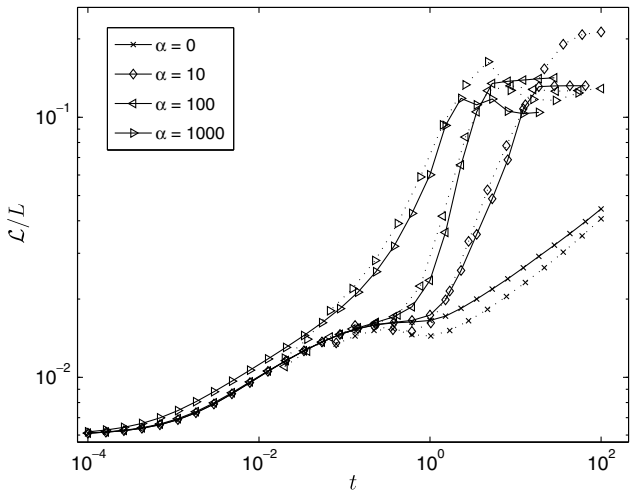

Fig. 4. Integral scale vs. time from 256^3 (solid) vs. 512^2 (dotted) simulations of spinodal decomposition of critical mixtures in a periodic box with $\Psi = 2.1$ for different values of α.

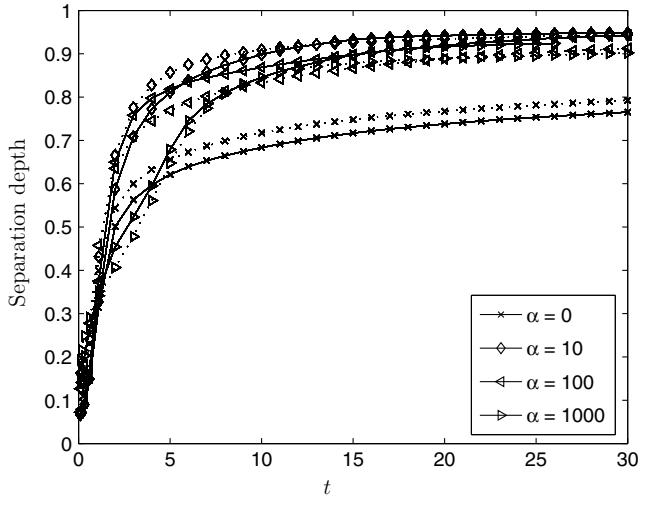

Fig. 5. Separation depth vs. time from 256^3 (solid) vs. 512^2 (dotted) simulations of spinodal decomposition of critical mixtures in a periodic box with $\Psi = 2.1$ for different values of α.

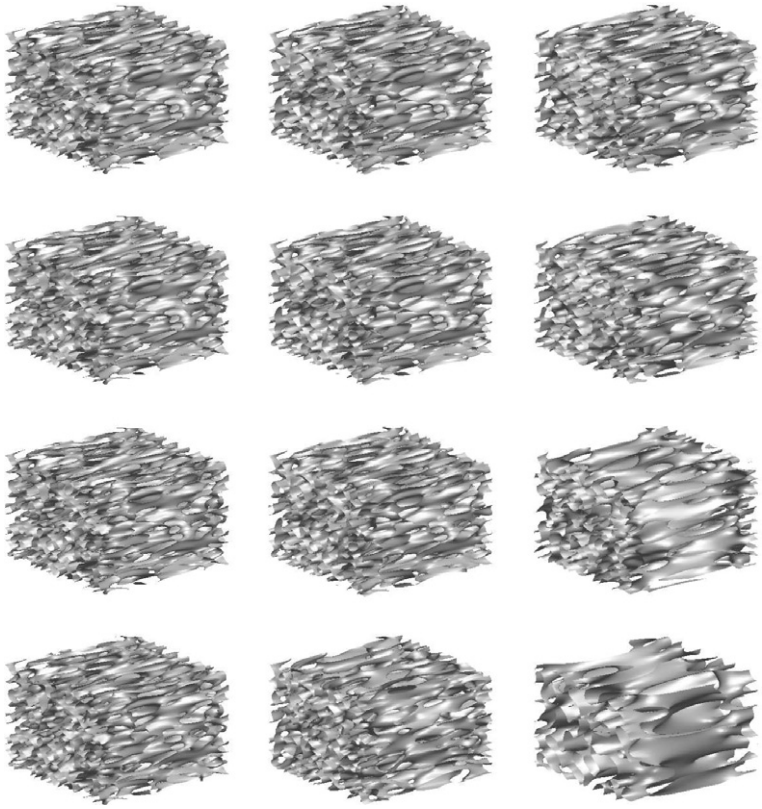

Fig. 6. Phase separation of a critical mixture (from $64 \times 65 \times 64$ simulations with $\phi_0 = 0.5$ and $\Psi = 2.1$) in a channel at different nondimensional times $t = 0.5$, 1 and 2, with $\alpha = 0$, 10, 10^2 and 10^3 from top to bottom.

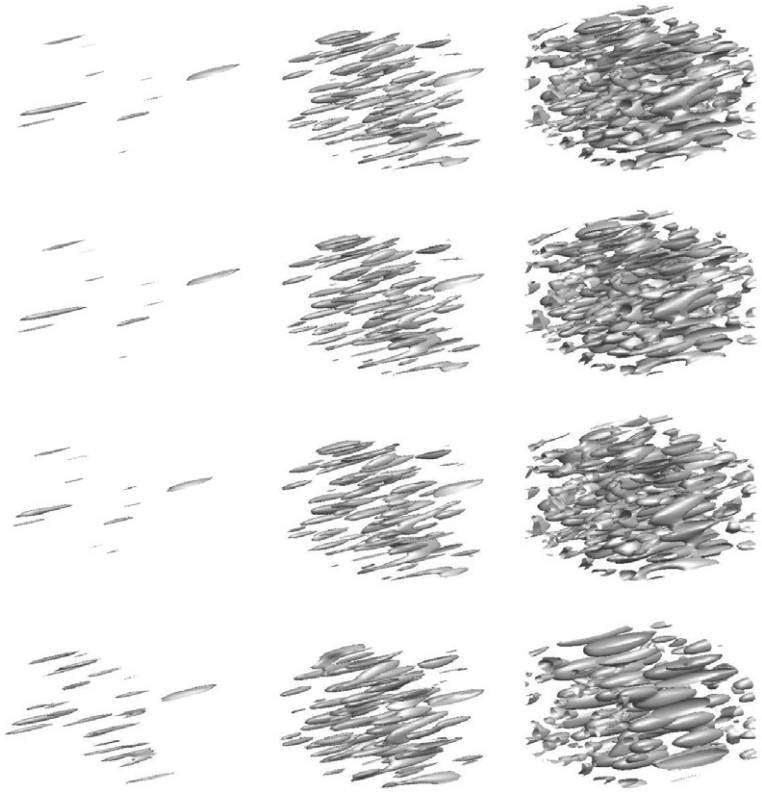

Fig. 7. Phase separation of an off-critical mixture (from $64 \times 65 \times 64$ simulations with $\phi_0 = 0.45$ and $\Psi = 2.1$) in a channel at different nondimensional times $t = 0.5$, 1 and 2, with $\alpha = 0$, 10, 10^2 and 10^3 from top to bottom.

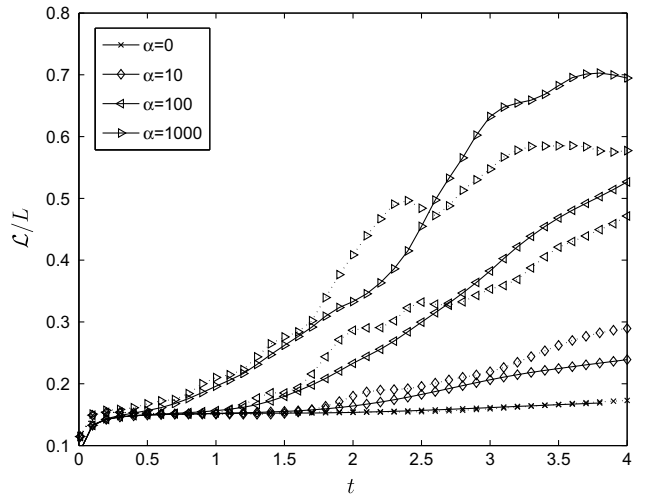

Fig. 8. Mean integral scale vs. time from 3D (solid) vs. 2D (dotted) simulations of spinodal decomposition of critical mixtures in a channel with $\Psi = 2.1$ for different values of α.

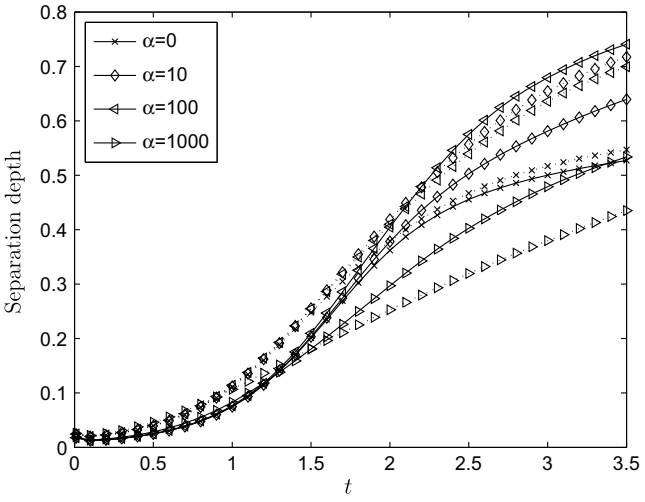

Fig. 9. Separation depth vs. time from 3D simulation (solid) vs. 2D (dotted) simulations of spinodal decomposition of critical mixtures in a channel with $\Psi = 2.1$ for different values of α.

5. Conclusions

In this paper we have shown results from 2D and 3D numerical simulations of spinodal decomposition in a periodic box and in a channel-like geometry. Spinodal patterns for critical and off-critical mixtures have been presented as a function of the "fluidity" parameter. We have shown remarkable agreement for separation statistics (such as, e.g., the separation depth and the integral scale of the radial pair-correlation function) in a periodic box, which supports the conclusion that 2D simulations are able to quantitatively capture the main features of 3D spinodal decomposition.

A new numerical method has been presented for integrating the coupled Stokes and Cahn–Hilliard equations in a plane channel. This method is based on the vertical-velocity/vertical-vorticity formulation of Kim et al. (1987) and therefore it is highly efficient in contrast to numerical schemes for the Navier–Stokes/Cahn–Hilliard system previously shown in the literature, which require a pressure Poisson solver.

Preliminary results from numerical simulations in a channel would suggest that the agreement between 2D and 3D results that was previously observed for the separation statistics in a periodic box deteriorates for spinodal decomposition in a channel.

Acknowledgements

Support and computational resources made available by the Center for Turbulence Research, Stanford University, are gratefully acknowledged. RM gratefully acknowledges support by MIUR (Ministero Italiano dell'Università e della Ricerca).

References

Anderson, D.M., McFadden, G.B., Wheeler, A.A., 1998. Diffuse interface methods in fluid mechanics. Annu. Rev. Fluid Mech. 30, 139–165.
Antanovskii, L.K., 1995. A phase-field model of capillarity. Phys. Fluids 7, 747–753.
Antanovskii, L.K., 1996. Microscale theory of surface tension. Phys. Rev. E 54, 6285–6290.
Badalassi, V.E., Ceniceros, H.D., Banerjee, S., 2003. Computation of multiphase systems with phase field models. J. Comput. Phys. 190, 371–397.
Beretta, G.P., Gyftopoulos, E.P., 2005. Thermodynamics: Foundations and Applications. Dover Publications, New York.
Berti, S., Boffetta, G., Cencini, M., Vulpiani, A., 2005. Turbulence and coarsening in active and passive binary mixtures. Phys. Rev. E 95, 224501.
Cahn, J.W., Hilliard, J., 1958. Free energy of a nonuniform system. I. Interfacial free energy. J. Chem. Phys. 28, 258–267.
Cahn, J.W., Hilliard, J., 1959. Free energy of a nonuniform system: III. Nucleation in a two-component incompressible fluid. J. Chem. Phys. 31, 688–699.
Caneba, G., Chen, Y.-L., Solc, K., 2002. Computer simulation of spinodal decomposition in one, two, and three dimensions. Presented at the A.I.Ch.E. Annual Meeting, Indianapolis, IN.
Canuto, C., Hussaini, M., Quarteroni, A., Zang, T., 1988. Spectral Methods in Fluid Dynamics. Springer, New York.
Colombani, J., Bert, J., 2004. Toward a complete description of nucleation and growth in liquid-liquid phase separation. J. Non-Equilib. Thermodyn. 29, 389–395.
Furukawa, H., 1985. Effect of inertia on droplet growth in a fluid. Phys. Rev. A 31, 1103–1108.
Guenoun, P., Gastaud, R., Perrot, F., Beysens, D., 1987. Spinodal decomposition patterns in an isodensity critical binary fluid. Phys. Rev. A 36, 4876–4890.
Gunton, J.D., 1999. Homogeneous nucleation. J. Stat. Phys. 95, 903–923.
Gunton, J.D., San Miguel, M., Sahni, P.S., 1983. The dynamics of first-order phase transitions. In: Domb, C., Lebowitz, J.L. (Eds.), Phase Transition and Critical Phenomena, vol. 8. Academic Press, pp. 267–466.
Gupta, R., Mauri, R., Shinnar, R., 1999. Phase separation of liquid mixtures in the presence of surfactants. Ind. Eng. Chem. Res. 38, 2418–2424.
Hohenberg, P.C., Halperin, B.I., 1977. Theory of dynamic critical phenomena. Rev. Mod. Phys. 49, 435–479.
Horvay, G., Cahn, J.W., 1961. Dendritic and spheroidal growth. Acta Met. 9, 695–705.
Iovieno, M., Cavazzoni, C., Tordella, D., 2001. A new technique for a parallel dealiased pseudo-spectral Navier–Stokes code. Comput. Phys. Commun. 141, 365–374.
Jacqmin, D., 2000. Contact line dynamics of a diffuse fluid interface. J. Fluid Mech. 402, 57–88.
Jasnow, D., Vinals, J., 1996. Coarse-grained description of thermo-capillary flow. Phys. Fluids 8, 660–669.
Kawasaki, K., 1970. Kinetic equations and time correlation functions of critical fluctuations. Ann. Phys. 61, 1–56.
Kendon, V.M., 2000. Scaling theory of three-dimensional spinodal turbulence. Phys. Rev. E 61, R6071–R6074.
Kendon, V.M., Cates, M.E., Pagonabarraga, I., Desplat, J.-C., Bladon, P., 2001. Inertial effects in three-dimensional spinodal decomposition of a symmetric binary fluid mixture. J. Fluid Mech. 440, 147–203.
Kim, J., Moin, P., Moser, R., 1987. Turbulence statistics in fully developed channel flow at low Reynolds number. J. Fluid Mech. 177, 133–166.
Lamorgese, A.G., Mauri, R., 2002. Phase separation of liquid mixtures. In: Continillo, G. et al. (Eds.), Nonlinear Dynamics and Control in Process Engineering. Springer, Rome, pp. 139–152.
Lamorgese, A.G., Mauri, R., 2005. Nucleation and spinodal decomposition of liquid mixtures. Phys. Fluids 17, 034107.
Lamorgese, A., Mauri, R., 2006. Mixing of macroscopically quiescent liquid mixtures. Phys. Fluids 18, 044107.
Landau, L.D., Lifshitz, E.M., 1953. Fluid Mechanics. Pergamon Press, New York (Chapter 6).
Langer, J.S., 1980. Kinetics of metastable states. In: Garrido, L. (Ed.), Systems Far from Equilibrium. Lecture Notes in Physics No. 132. Springer, pp. 12–47.
Langer, J.S., Schwartz, A.J., 1980. Kinetics of nucleation in near-critical fluids. Phys. Rev. A 21, 948–958.
Le Bellac, M., 1991. Quantum and Statistical Field Theory. Clarendon Press, Oxford, UK (Chapters 2 and 3).
Lele, S., 1992. Compact finite-difference schemes with spectral-like resolution. J. Comput. Phys. 103, 16–42.
Lifshitz, E.M., Pitaevskii, L.P., 1984. Physical Kinetics. Pergamon Press, New York.

Lowengrub, J., Truskinovsky, L., 1998. Quasi-incompressble Cahn-Hilliard fluids and topological transitions. Proc. Roy. Soc. A 454, 2617–2654.
Mauri, R., Shinnar, R., Triantafyllou, G., 1996. Spinodal decomposition in binary mixtures. Phys. Rev. E 53, 2613–2623.
Peyret, R., 2000. Introduction to high-order approximation methods for computational fluid dynamics. In: Peyret, R., Krause, E. (Eds.), Turbulent Flow Computations, Vol. 395. CISM, pp. 1–79.
Poesio, P., Cominardi, G., Lezzi, A., Mauri, R., Beretta, G.P., 2006. Effects of quenching rate and viscosity on spinodal decomposition. Phys. Rev. E 74, 011507.
Prusty, M., Keestra, B., Goossens, J., Anderson, P., 2007. Experimental and computational study on structure development of PMMA/SAN blends. Chem. Eng. Sci. 62, 1825–1837.
Santonicola, G.M., Mauri, R., Shinnar, R., 2001. Phase separation of initially non-homogeneous liquid mixtures. Ind. Eng. Chem. Res. 40, 2004–2010.
Siggia, E., 1979. Late stages of spinodal decomposition in binary mixtures. Phys. Rev. A 20, 595–605.
Tanaka, H., Araki, T., 1998. Spontaneous double phase separation induced by rapid hydrodynamic coarsening in two-dimensional fluid mixtures. Phys. Rev. Lett. 81, 389–392.
Valls, O.T., Farrell, J.E., 1993. Spinodal decomposition in a three-dimensional fluid model. Phys. Rev. E 47, R36–R39.
Van der Waals, J.D., 1894. The thermodynamic theory of capillarity under the hypothesis of a continuous variation of density. Z. Phys. Chem. Stöchiom. Verwandtschaftsl. 13, 657 (translated and reprinted in J. Stat. Phys. 20, 200–244 (1979)).
Vladimirova, N., Malagoli, A., Mauri, R., 1998. Diffusion driven phase separation of deeply quenched mixtures. Phys. Rev. E 58, 7691–7699.
Vladimirova, N., Malagoli, A., Mauri, R., 1999a. Diffusiophoresis of two-dimensional liquid droplets in a phase-separating system. Phys. Rev. E 60, 2037–2044.
Vladimirova, N., Malagoli, A., Mauri, R., 1999b. Two-dimensional model of phase segregation in liquid binary mixtures. Phys. Rev. E 60, 6968–6977.